Mechanistic Features and Structure of the Nitrogenase α-Gln^{195} MoFe Protein[†,‡]

Morten Sørlie,[§] Jason Christiansen,[⊥] Brian J. Lemon,[#] John W. Peters,[#] Dennis R. Dean,[⊥] and Brian J. Hales*[,§]

Department of Chemistry, Louisiana State University, Baton Rouge, Louisiana 70803-1804 and Department of Biochemistry, Virginia Tech, Blacksburg, Virginia 24061-0346 and Department of Chemistry and Biochemistry, Utah State University, Logan, Utah 84322

Received June 19, 2000; Revised Manuscript Received November 14, 2000

ABSTRACT: EPR signals observed under CO and C_2H_2 during nitrogenase turnover were investigated for the α-Gln^{195} MoFe protein, an altered form for which the α-His^{195} residue has been substituted by glutamine. Under CO, samples show $S = 1/2$ hi- and lo-CO EPR signals identical to those recognized for the wild-type protein, whereas the $S = 3/2$ signals generated under high CO/high flux conditions differ. Previous work has revealed that the EPR spectrum generated under C_2H_2 exhibits a signal (S_{EPR1}) originating from the FeMo-cofactor having two or more bound C_2H_2 adducts and a second signal (S_{EPR2}) arising from a radical species [Sørlie, M., Christiansen, J., Dean, D. R., and Hales, B. J. (1999) *J. Am. Chem. Soc. 121*, 9457−9458]. Pressure-dependent studies show that the intensity of these signals has a sigmoidal dependency at low pressures and maximized at 0.1 atm C_2H_2 with a subsequent decrease in steady-state intensity at higher pressures. Analogous signals are not recognized for the wild-type MoFe protein. Analysis of the principal *g*-factors of S_{EPR2} suggests that it either represents an unusual metal cluster or is a carboxylate centered radical possibly originating from homocitrate. Both S_{EPR1} and S_{EPR2} exhibit similar relaxation properties that are atypical for $S = 1/2$ signals originating from Fe−S clusters or radicals and indicate a coupled relaxation pathway. The α-Gln^{195} MoFe protein also exhibits these signals when incubated under turnover conditions in the presence of C_2H_4. Under these conditions, additional inflections in the *g* 4−6 region assigned to ground-state transitions of an $S = 3/2$ spin system are also recognized and assigned to turnover states of the MoFe protein without C_2H_4 bound. The structure of α-Gln^{195} was crystallographically determined and found to be virtually identical to that of the wild-type MoFe protein except for replacement of an NH−S hydrogen bond interaction between FeMo-cofactor and the imidazole side chain of α-His^{195} by an analogous interaction involving Gln.

Biological nitrogen fixation is catalyzed by nitrogenase, a complex metalloenzyme composed of two separately purifiable components called the Fe protein and the MoFe protein (*1*). The Fe protein is a homodimer ($M_r \sim 64\,000$) containing two nucleotide binding sites and a [4Fe-4S] cluster that bridges the identical subunits (*2*). The MoFe protein is an $\alpha_2\beta_2$ heterotetramer ($M_r \sim 240\,000$) that contains two novel metalloclusters, the [8Fe-7S] P cluster (*3*) and the [7Fe-9S-Mo + homocitrate] FeMo-cofactor (*4*, *5*). One P cluster is located at each MoFe protein α*β*-subunit interface, and one FeMo-cofactor is located within each α-subunit. In addition to the physiological substrate, dinitrogen, nitrogenase is also able to reduce protons and a variety of other multiply bonded small molecules, the most commonly studied one being C_2H_2 (*6*−*8*). During catalytic activity, in vitro, the two component proteins associate and a single electron is transferred from the Fe protein to the MoFe protein P-cluster and ultimately to the FeMo-cofactor,[1] where substrate reduction takes place (*9*). For each electron transferred, at least two molecules of MgATP are hydrolyzed at the Fe protein (*10*). After electron transfer and MgATP hydrolysis, the component proteins dissociate. This process is repeated until sufficient reducing equivalents are accumulated within the MoFe protein so that substrate can be reduced and the enzyme can return to the resting state (*11*).

Because the FeMo-cofactor provides the substrate reduction site, its structure and reactivity has received considerable attention (*1*−*3*). Neither isolated FeMo-cofactor nor FeMo-cofactorless MoFe protein exhibit any substrate reduction

[†] Support provided by the U.S. Department of Agriculture (Grant Nos. 99-35305-8645 to BJH and 98-03559 to J.W.P.) and the National Institutes of Health (Grant No. R01-GM59087 to D.R.D.).

[‡] Crystal Structure: Coordinates have been submitted to the RCSB Protein Data Base accession code 1FP4.

* Corresponding author. Telephone: (225) 578-4694. Fax: (225) 578-3458. E-mail: bhales@lsu.edu.

[§] Louisiana State University.

[⊥] Virginia Tech.

[#] Utah State University.

[1] Abbreviations: α-Gln^{195}, variant MoFe protein for which His at the α-195 position has been substituted by Gln; FeMo-cofactor, $MoFe_7S_9$-homocitrate cluster serving as the putative active site in the MoFe protein; lo-CO, rhombic $S = 1/2$ EPR cofactor signal generated during Mo-nitrogenase turnover in the presence of low concentrations of CO; hi-CO, axial $S = 1/2$ EPR cofactor signal generated during Mo-nitrogenase turnover in the presence of high concentrations of CO; hi(5)-CO, rhombic $S = 3/2$ EPR signal generated during Mo-nitrogenase turnover in the presence of high concentrations of CO and high electron flux; S_{EPR1}, rhombic $S = 1/2$ EPR cofactor signal generated during Mo-nitrogenase turnover with the α-Gln^{195} protein in the presence of C_2H_2; S_{EPR2}, nearly isotropic $S = 1/2$ EPR radical signal generated during Mo-nitrogenase turnover with the α-Gln^{195} protein in the presence of C_2H_2; S_{EPR3}, negative inflection of unknown origin generated during Mo-nitrogenase turnover with the α-Gln^{195} protein in the presence of C_2H_2.

10.1021/bi0013997 CCC: $20.00
Published on Web 01/19/2001

activity (*12*), suggesting that specific cofactor−peptide interactions are crucial for effective substrate binding and reduction. In previous work, we gained insight about the functioning of nitrogenase by characterizing an altered *Azotobacter vinelandii* MoFe protein that has the α-subunit His[195] residue substituted by glutamine (*13*). This residue normally provides a hydrogen bond through the Nϵ of its imidazole group to a bridging S of FeMo-cofactor. The altered MoFe protein, designated "α-Gln[195] MoFe protein", does not significantly reduce N_2 but is able to reduce C_2H_2 with kinetic parameters similar to those of the wild-type enzyme. Even though N_2 cannot serve as an effective substrate for the α-Gln[195] MoFe protein, it remains an inhibitor of both C_2H_2 and proton reduction, indicating that N_2 is able to occupy the active site without being reduced.

Although there are many known substrates for nitrogenase, relatively little is known about the nature of their binding and reduction at the FeMo-cofactor. Under enzymatic turnover, the potent inhibitor, CO, has been shown to produce two different, intense EPR signals that depend on the partial pressure of CO (P_{CO}) in the system (*14*−*16*). However, until recently, EPR signals of similar intensity have not been observed for any of the reducible substrates. We previously communicated results showing that the α-Gln[195] MoFe protein produces a strong EPR signal in the $g \sim 2$ region during enzymatic turnover in the presence of the one of the best studied substrates, C_2H_2 (*17*). This signal comprises three different species including: a rhombic signal (g = [2.12, 1.98, 1.95] designated g 2.12 or S_{EPR1}) assigned to the FeMo-cofactor with bound C_2H_2 adducts, a nearly isotropic radical signal centered at $g = 2.00$ (designated g 2.00 or S_{EPR2}) and a single, minor inflection at $g = 1.97$ (designated g 1.97 or S_{EPR3}). Recent ENDOR results confirm the assignment of S_{EPR1} and show at least two C_2H_2 adducts bound to the cofactor (*18*). In this paper, we examine the nature and behavior of S_{EPR1} and S_{EPR2} and report on the crystal structure determined for the α-Gln[195] MoFe protein.

MATERIALS AND METHODS

Cell Growth and Protein Purification. *A. vinelandii* cells were grown at 30 °C in a 150 L custom-built fermentor (W. B. Moore, Inc. Easton, PA) in modified Burk's medium containing 10 mM urea as the sole nitrogen source (*19*, *20*). Cultures were sparged with pressurized air (80 L/min at 5 psi) and agitated at 125 rpm. When the cell density reached 220 Klett units (red filter), cells were derepressed for *nif* gene expression by concentration (6-fold) using a custom-built AG Technologies tangential-flow concentrator and resuspended in modified Burk's medium with no added nitrogen. Harvested cells were stored at −80 °C until used. All protein manipulations were performed under anaerobic conditions maintained using either a Schlenk apparatus (*21*) or an anaerobic glovebox.

The α-Gln[195] MoFe protein was purified using a combination of immobilized metal-affinity chromatography (IMAC) and DEAE-Sepharose anion exchange chromatography as previously described (*22*). Protein was quantified using a modified biuret assay with bovine serum albumin as the standard (*23*), and protein purity was monitored by SDS−PAGE electrophoresis (*24*). The final purified product was pelleted and stored in liquid nitrogen until used. Approximately 360 g of cells (wet weight) was processed for each purification, and yields were approximately 1.1 g of purified α-Gln[195] MoFe protein per purification.

Assays. Nitrogenase assays were performed as previously described (*13*). Samples were incubated for 8 min with gentle shaking in a 30 °C water bath, and the reaction was terminated by addition of 250 μL of 0.4 M EDTA solution. H_2 production was monitored by injection of 200 μL of the gas phase into a Shimadzu GC-14 equipped with a Supelco 80/100 molecular sieve 5A column and a TCD detector. The α-Gln[195] MoFe protein exhibited specific activity comparable to what has been observed in previous studies (*13*).

Turnover EPR Samples. Unless otherwise noted, turnover samples consisted of 20 μM Fe protein, 100 μM α-Gln[195] MoFe protein, 0.1 atm C_2H_2, 10 mM ATP, 25 mM $MgCl_2$, 20 mM $Na_2S_2O_4$, and 50 mM TES-KOH pH 7.4. Prior to the addition of the Fe protein to initiate turnover, the other components of the above mixture were preincubated at 30 °C under an atmosphere containing either C_2H_2 or C_2H_4 (in argon) for 20 min. Following initiation of turnover by the addition of Fe protein, a 300 μL sample was transferred to an EPR tube where it was rapidly frozen in liquid N_2. The interval between turnover initiation and final freezing was approximately 2 min.

EPR spectra were recorded with a Bruker ER 300D spectrometer interfaced to a Bruker 1600 computer for data storage and manipulations. An Oxford Instruments ESR-900 helium flow cryostat positioned in a TE_{102} cavity was used to attain cryogenic temperatures. Temperatures were controlled and monitored using an Oxford Instruments model ITC4 temperature controller with a digital readout. Spin concentration determinations were performed on the spectrometer computer by double integration of the spectral envelope or isolated peaks using Cu(II)EDTA as a spin standard. All spin concentration determinations were performed at T ≥ 10 K to avoid saturation effects often encountered with Cu(II)EDTA at lower temperatures (*25*).

Values for D (the axial zero-field splitting parameter) were determined by curve-fitting Boltzmann distribution expressions for the relative populations of the doublets in question to Curie law corrected spectral areas recorded in temperature-dependent depopulation experiments (*26*). EPR spectral assignments for half-integer spin systems were affected by numerical determination of possible g-factors in the weak-field limit using the computer program RHOMBO (*27*).

Crystallization. For crystallization, the α-Gln[195] MoFe protein [lacking the seven tandem histidine residues at the C-terminus of the α-subunit, *A. vinelandii* strain DJ540 (*13*)] was equilibrated with 50 mM Tris, pH 8.0, buffer and 350 mM NaCl by passing the protein over a preequilibrated S-200 Sephacryl gel filtration column prior to crystallization. The protein was crystallized using the microcapillary batch diffusion method with a 30% PEG 400, 0.1 M Tris, pH 8.0, buffer and 0.2 M Na_2MoO_4 precipitation solution. Crystals appeared in approximately 1−2 weeks and are on the average $0.2 \times 0.6 \times 1.0$ mm^3. The α-Gln[195] MoFe protein crystallized in the same monoclinic ($P2_1$) space group with similar unit cell parameters as the previously characterized native MoFe protein (Table 1) (*5*).

The protein crystals were flash cooled in liquid nitrogen on rayon loops and kept under a continuous liquid nitrogen stream during data collection. Data were collected using a

Table 1: Data and Refinement Statistics

Data Statistics	
a (Å)	107.2
b (Å)	130.2
c (Å)	80.4
β (°)	111.2
resolution range (Å)	20.0−2.5
observations	403283
unique reflections	63058
R_{merge} (%)[b]	8.2 (25.2)[a]
completeness (%)	88.8 (60.0)[a]
Refinement Statistics	
resolution range (Å)	20.0−2.5
total reflections ($F > 1\sigma F$)	59345
R_{cryst} (%)	18.2
R_{free} (%)[c]	23.9
rms of bond distances (Å)	0.010
rms of bond angles (°)	2.50

[a] Statistics for the highest-resolution shell (2.54−2.50 Å) are indicated in parentheses. [b] $R_{merge} = \Sigma_{hkl}[\Sigma_i(|Ihkl,i - \langle Ihkl\rangle|]/\Sigma hkl,i\langle Ihkl\rangle$. [c] 2988 reflections were used in the calculation of R_{free}.

Rigaku RU200 X-ray generator and a Raxis II imaging plate detector. The data were processed using DENZO and SCALEPACK (*28*). Limited model fitting was accomplished using O (*29*) and refinement was done using X-PLOR (*30*) with simulated annealing refinement and an annealing temperature of 4000 K for randomization and cross-validation.

RESULTS AND DISCUSSION

Integrity of the Electronic Structure of the Metal Clusters in the α-Gln[195] MoFe Protein. As described for the crystal structure below, the Gln[195] MoFe protein arises from a single amino acid substitution in the immediate vicinity of the FeMo cofactor (Figure 1). Before interpreting the spectroscopic results obtained in the presence of C_2H_2 or C_2H_4, it is important to determine the magnitude of the perturbation this substitution has on the electronic environment of both the FeMo cofactor and the P cluster. Alterations in electronic features can be easily monitored by changes in the EPR spectrum. The FeMo cofactor is EPR-active in the as-isolated dithionite-reduced form of the protein. In this state, the α-Gln[195] MoFe protein exhibits a slight rhombic shift in the FeMo cofactor $S = 3/2$ signal changing the *g*-factors [4.36, 3.64, 2.00] when compared to the values [4.33, 3.77, 2.00] for the wild-type MoFe protein (*31*). In contrast, EPR spectra of the CO-bound form of the FeMo cofactor shown as lo-CO (0.01 atm CO in Ar) and hi-CO (1.0 atm CO) (Figure 2, panel A) are identical for both proteins (*14*−*16*)**.** This is true even though the α-Gln[195] MoFe is approximately 10× more sensitive to inhibition by CO when compared to the wild type MoFe protein. Because others have recently reported that the α-Gln[195] substitution has only a minor effect on the CO interacton (*32*, *33*), we also characterized an α-Gln[195] MoFe protein from a newly constructed strain and reconfirmed our original kinetic results (*13*).

Under 1.0 atm CO and high flux conditions, a second signal (other than hi-CO) has been shown to be generated in the $g \sim 5$ region for the wild-type enzyme and identified as an $S = 3/2$ state preliminarily associated with a second form of the CO-bound cofactor (*34*). Because this state occurs in the $g \sim 5$ region and requires high CO concentrations and high electron flux, it will be referred to as hi(5)-CO to show that it differs from the normal $S = 1/2$ hi-CO state in the *g*-2 region. Unlike lo-CO and hi-CO, hi(5)-CO has spectral parameters different in the α-Gln[195] mutant ($g = 5.87$ and 4.94; $E/D = 0.17$ and $D = 1.25$ cm^{-1}) as compared to the wild type ($g = 5.88$ and 4.70; $E/D = 0.12$ and $D = 0.43$ cm^{-1}) proteins (Figure 2, panel B) thus strengthening the hypothesis that it originates at the FeMo cofactor. Estimated spin quantitations of all EPR-active signals are shown in Table 2.

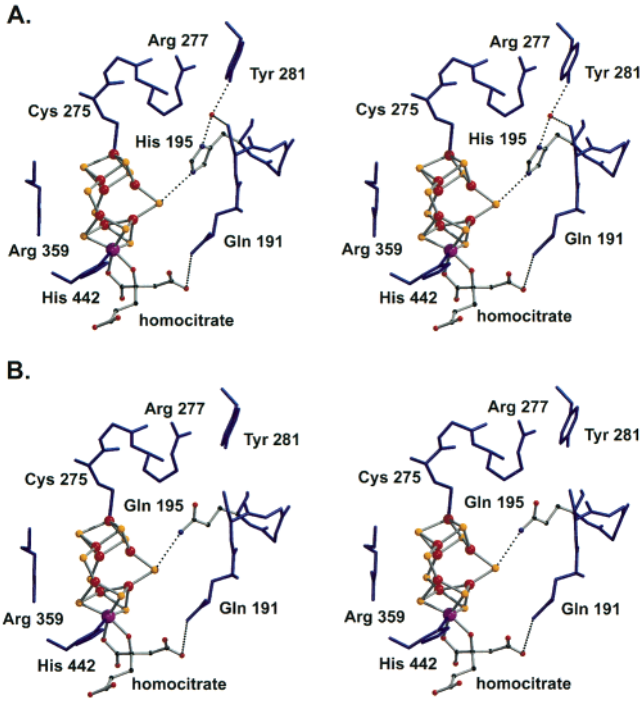

FIGURE 1: Stereoviews of the comparison of the crystal structures of the FeMo-cofactor and surrounding amino acids for the α-Gln[195] (B) and wild-type (A) MoFe proteins.

Changes in the electronic structure of the P clusters can similarly be monitored by EPR spectroscopy. In the as-isolated state of the MoFe protein, the P-clusters are diamagnetic but become paramagnetic and EPR-active when oxidized to states P^+ ($S = 1/2$ and $S = 5/2$ states) (*26*) or P^{2+} ($S = 3$ or 4 state) (*26*, *27*, *35*, *36*). Spectra of half-integer states are often sharper and better defined than those of integer states and, as such, are more sensitive indicators of small electronic changes. Thus, the P^+ state of the α-Gln[195] MoFe protein was generated for comparison with the wild-type MoFe protein by indigodisulfonate treatment (*26*). The EPR spectrum of the partially oxidized protein (results not shown) exhibited the characteristic $S = 5/2$ and 1/2 signals of P^+ that are identical to the spectrum previously reported for the wild-type enzyme (*26*). Therefore, as expected, the α-Gln[195] substitution only slightly perturbs the electronic environment about the cofactor, as observed by the changes in the as-isolated and hi(5)-CO spectra, while exerting no detectable effect on the characteristic P cluster spectra.

Enzymatic Turnover of the α-Gln[195] MoFe Protein in the Presence of C_2H_2. When prepared under turnover conditions in the presence of 0.1 atm C_2H_2, the α-Gln[195] MoFe protein has been shown to give rise to a strong EPR spectrum in the *g*-2 region (Figure 3) (*17*). This spectrum can be decomposed into three species, S_{EPR1}, S_{EPR2}, and S_{EPR3}. S_{EPR1} ($g = [2.12,$

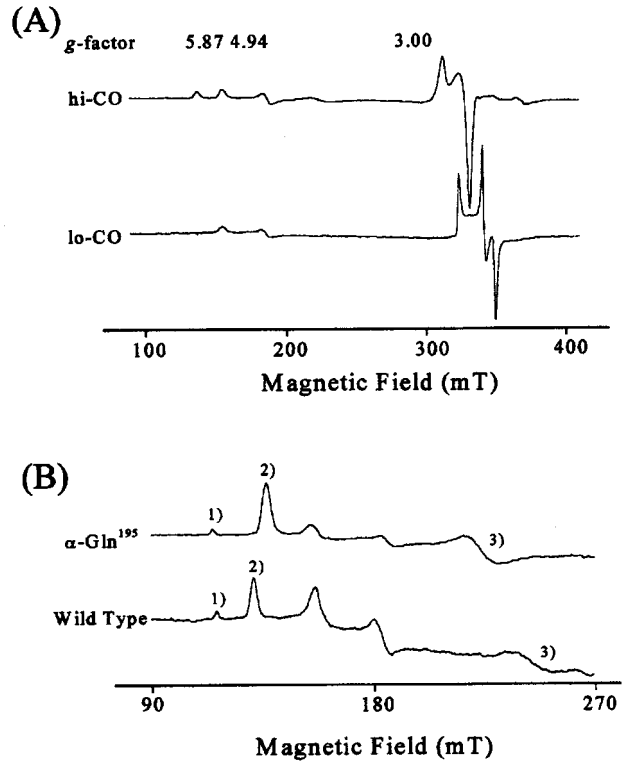

FIGURE 2: (A) The EPR spectra of α-Gln[195] during enzymatic turnover in the presence of 1.0 atm CO (top) and 0.001 atm CO (bottom) showing hi-CO and lo-CO signals, respectively, in the $g = 2$ region. Also shown at low field are the small inflections associated with the $S = 3/2$ signal of the as-isolated form of the FeMo-cofactor; temperature = 9 K. (B) EPR spectra of α-Gln[195] and wild-type enzymes during turnover in the presence of 1 atm of CO showing the three lowest-field inflections labeled 1, 2, and 3 of hi(5)-CO. These inflections correspond to the excited-state doublet (1) and the ground-state doublet (2 and 3) of an $S = 3/2$ spin system (see Table 2). Additional inflections between 2 and 3 arise from small concentrations of the as-isolation form of the FeMo-cofactor; temperature = 4 K. Experimental conditions for all spectra: [Fe protein]/[MoFe protein] = [20 μM]/[100 μM] = 1:5; [$MgCl_2$] = 25 mM; [$Na_2S_2O_4$] = 20 mM; 50 mM TES-KOH, pH = 7.4. Spectrometer parameters: microwave frequency = 9.45 GHz; microwave power = 20 mW; modulation amplitude = 0.5 mT.

1.98, 1.95]) and has been identified as arising from at least two C_2H_2 adducts bound to the FeMo-cofactor (*17*, *18*). S_{EPR2} (isotropic $g = 2.00$) is a radical signal, and S_{EPR3} (minor shoulder at $g = 1.97$) is of unknown origin (*17*). Spin quantitation (Table 2) at 12 K shows that S_{EPR1} (and S_{EPR3}; these two species overlap and cannot be separately integrated) represent about 22% of the total cofactor concentration, while S_{EPR2} and the $S = 3/2$ signal from the FeMo-cofactor represent another 1 and 13%, respectively.

Paramagnetic centers can also be characterized in terms of their spin relaxation properties. In general, EPR spectra of isolated radicals are easily observed at room temperatures but exhibit significant power saturation when the temperature is lowered to near liquid He. On the other hand, typical $S = 1/2$ signals of Fe−S clusters require low temperatures (20−12 K) to suppress the effects of relaxation broadening but demonstrate power saturation effects at lower temperatures. As such, the relaxation properties of S_{EPR1} and S_{EPR2} are atypical for $S = 1/2$ Fe−S centers or radical signals since they both are only observed without broadening at 4 K and exhibit significant line broadening when the temperature is

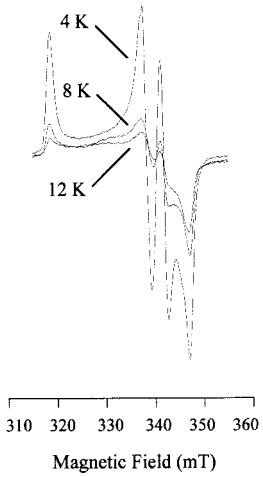

FIGURE 3: Temperature dependence of the EPR spectrum of α-Gln[195] during enzymatic turnover in the presence of 0.1 atm C_2H_4. Spectra were recorded at 5 mW power and 4, 8, and 12 K illustrating the broadening at the higher temperature. S_{EPR1} and S_{EPR2} (but not S_{EPR3} which can still be observed as a negative inflection at 16 K) have the strongest temperature dependency and are almost undetectable at 12 K. For example, note stronger contribution of S_{EPR3} to spectrum at 12 K as compared to at 4 K.

increased to only 8 K (Figure 3). In fact, at temperatures higher than 12 K S_{EPR1} and S_{EPR2} are virtually undetectable. Furthermore, power-dependence studies (Figures 4 and 5) at 4 K show that S_{EPR1} and S_{EPR2} display similar saturation behavior suggesting that they have a coupled relaxation pathway. If S_{EPR1} and S_{EPR2} were separated by a large distance (>30 Å) no coupling would occur, and each would relax independent of the other. At short distances, the faster relaxing species would initially increase the relaxation rate of the slower species, but not vice versa. However, in our system both S_{EPR1} and S_{EPR2} show enhanced relaxation rates over what is typically observed for $S = 1/2$ centers. Furthermore, the concentrations of S_{EPR1} and S_{EPR2} are not equal, as would be required for both species to be simultaneously present. One possible explanation is that S_{EPR1} exhibits fast relaxation atypical of $S = 1/2$ metal clusters, and we are observing a mixture of protein with either S_{EPR1} by itself or coupled S_{EPR1} and S_{EPR2} species.

The dependency of a steady-state signal on substrate concentration is often used to determine the number of binding sites. When the signal amplitude of S_{EPR1} is plotted versus the percentage of C_2H_2, a sigmoidal curve is produced up to 10% C_2H_2 where the signal maximizes and subsequently decreases at higher percentages (Figure 6). The reason for this decrease at high pressures is unknown but may arise from and increase in the rate of decay of the paramagnetic state at elevated pressures. It should be noted that no major changes in the shape of the composite EPR signal occurred over this concentration range. The sigmoidal behavior at low C_2H_2 concentrations (see insert in Figure 6) suggests multiple enzyme binding events. The number of binding sites can be approximated with a Hill-type plot. Specifically, if n C_2H_2 molecules are required to generate the observed EPR signal ([S_{EPR1}]), then

$$\log\{[S_{EPR1}]/([S_{EPR1}]_{max} - [S_{EPR1}])\} = n \log[C_2H_2] \quad (1)$$

where $[S_{EPR1}]_{max}$ is the maximum EPR intensity. Taking the value of $[S_{EPR1}]_{max}$ from the amplitude obtained at 10% C_2H_2

Table 2: EPR Detectable Signals During Turnover with α-Gln[195] MoFe-Protein

signal	*g*-factors[a]	*D* (cm^{-1})	*E*/*D*	%[b]	identity
		Under Ar			
$S = 3/2$	4.36, 3.64, 2.00	6.0	0.05	10	resting state of FeMo-cofactor
		Under CO (0.01 atm)			
$S = 3/2$	4.36, 3.64, 2.00	6.0	0.05	8	resting state of FeMo-cofactor
lo-CO	2.09, 1.97, 1.93	NA[c]	NA	10	FeMo-cofactor with one CO bound
		Under CO (1.0 atm)			
$S = 3/2$	4.36, 3.64, 2.00	6.0	0.05	8	resting state of FeMo-cofactor
hi-CO	2.17, 2.06, 2.06	NA	NA	26	FeMo-cofactor with two COs bound
hi(5)-CO	4.94, 3.00, 1.85, 5.87, (1.08), (0.91)	1.25	0.17	6	proposed $S = 3/2$ FeMo-cofactor state with CO bound different from hi-CO
		Under C_2H_2 (0.1 atm)			
$S = 3/2$	4.36, 3.64, 2.00	6.0	0.05	8	resting state of FeMo-cofactor
S_{EPR1}	2.12, 1.98, 1.95	NA	NA	22[d]	FeMo-cofactor with at least two C_2H_2 adducts bound
S_{EPR2}	2.007, 2.000, 1.992	NA	NA	1	homocitrate, aspartate or glutamate radical
S_{EPR3}	1.97[e]	NA	NA	(see S_{EPR1})	unknown
		Under C_2H_4 (1.0 atm)			
$S = 3/2$	4.36, 3.64, 2.00	6.0	0.05	17	resting state of FeMo-cofactor
S_{EPR1}	2.12, 1.98, 1.95	NA	NA	22[d]	FeMo-cofactor with at least two C_2H_2 adducts bound
S_{EPR2}	2.007, 2.000, 1.992	NA	NA	1	homocitrate, aspartate, or glutamate radical
S_{EPR3}	1.97[e]	NA	NA	(see S_{EPR1})	unknown
g 2.06	2.06, 1.94, 1.86	NA	NA	2	reduced Fe protein
$6 \geq g \geq 4$ signals					
g 5.92	5.92, (0.75), (0.66)	<0	0.11	4[f]	proposed ground-state $S = 3/2$ FeMo-cofactor signals without C_2H_2 adducts bound
g 5.76	5.76, (1.31), (1.06)	<0	0.21	4[f]	
g 5.45	5.45, 5.45, 5.45	NA	0.33	4[f]	
g 4.62	4.62, 3.30, (1.93)	>0	0.11	4[f]	

[a] *g*-factors in parentheses are predicted but not observed. [b] Percent of total FeMo-cofactor concentration. [c] NA = not applicable; $S = 1/2$ spin state does not have zero-field splitting parameters (*D*). [d] Represents % of S_{EPR1} and S_{EPR3}; these signals cannot be separately quantified due to the overlap of their signals. [e] Other *g*-factors of S_{EPR3} signal are not observed and cannot be predicted. [f] Represents combined % of all four $6 \geq g \geq 4$ signals.

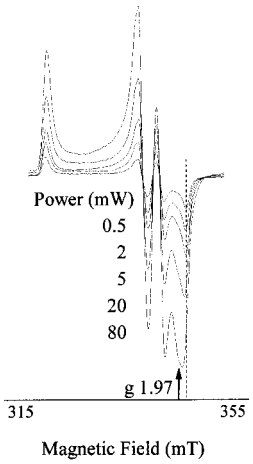

FIGURE 4: Microwave power dependence of the EPR signal observed at 4 K in the presence of 0.1 atm C_2H_2 and powers 0.5 to 80 mW. As power increases, $g = 1.95$ inflection of S_{EPR1} signal shifts toward $g = 1.97$ inflection of S_{EPR3} since the latter does not easily saturate.

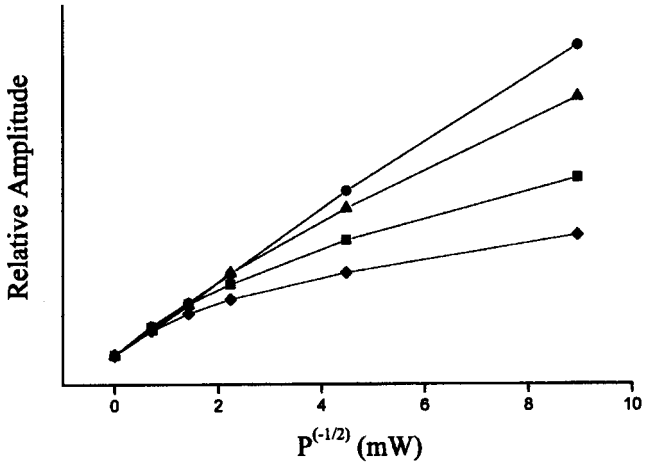

FIGURE 5: Saturation profiles at 4 K of S_{EPR1} (●), S_{EPR2} (▲), S_{EPR3} (■) and the EPR signal of the Fe protein (◆). The Fe protein has been included to represent the saturation behavior typically observed for a reduced Fe_4S_4 protien. Normalized signal amplitude is plotted versus the square root of the irradiating microwave power.

(Figure 6), a plot of the data (not shown) yields $n = 2$, suggesting that the S_{EPR1} signal represents two molecules of C_2H_2 adduct bound to the FeMo-cofactor. Since the amplitude of the signal decreases at pressures >0.1 atm, it is difficult to determine the actual signal maximum $([S_{EPR1}]_{max})_{Actual}$. Because $([S_{EPR1}]_{max})_{Actual} \geq ([S_{EPR1}]_{max})_{Observed}$ and $n_{Actual} \leq n_{Observed}$ according to eq 1, n_{Actual} cannot be greater than 2 and, therefore, most likely equals 2. It should be noted that the sigmoidal features for C_2H_2 interaction observed here on the basis of EPR is not reflected by detectable sigmoidal kinetics for substrate reduction. This is most likely because the substrate reduction activities are examining product formation, while the EPR experiment is examining possible intermediate states in product formation.

As previously shown in the study of CO inhibition of nitrogenase (*34*), electron flux can influence the formation of the lo-CO and hi-CO EPR signals. Because Fe protein is the obligate electron donor to the MoFe protein, the electron

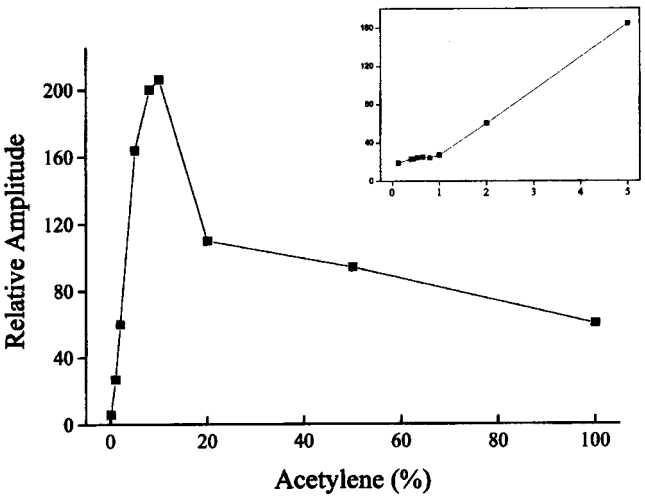

FIGURE 6: Dependence of the amplitude of S_{EPR1} on the C_2H_2 percentage in the gas phase. Inset shows the sigmoidal behavior in the low-pressure region.

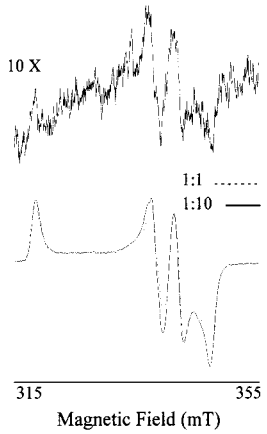

FIGURE 7: Dependence of the EPR spectrum on the [Fe protein]/[MoFe protein] component ratio (1:50, 1:5, and 1:1). Samples were rapidly frozen 2 min after initiation of the reaction. Note that S_{EPR1} and S_{EPR2} are present in all spectra and that the S_{EPR2}/S_{EPR1} ratio is slightly diminished in the spectrum recorded with a 1:1 component ratio. The absence of a detectable signal from the Fe protein suggests that most of that protein is in the diamagnetic oxidized state following electron transfer to the MoFe protein.

flux through the enzyme can be controlled by adjusting the component protein ratio ([Fe protein]/[MoFe protein]). Flux is maximized at a high Fe protein/MoFe protein ratio (typically, a component protein ratio ≥ 5:1). Turnover samples were prepared with different component protein ratios between 1:50 (very low electron flux) to 1:1 (moderate flux). Because of the high protein concentrations necessary to record EPR spectra, samples having component ratios above 1:1 could not be prepared. Spectra taken after 2 min at very low electron flux (Figure 7) represent the initially formed paramagnetic species because under these conditions the system does not have enough time to reach steady-state. Under these low flux conditions, the C_2H_2-induced signal exhibits the same general features of the signal at steady state but with much lower intensity. It is especially important to note that both S_{EPR1} and S_{EPR2} are present and in approximately the same ratio as observed at higher flux, suggesting that one species is not a mechanistic precursor to the other. All of the spectra recorded at higher electron flux were the same with the exception of the spectra at a component ratio of 1:1 where the relative amount of S_{EPR2} is slightly lower (Figure 7) than that observed at lower flux.

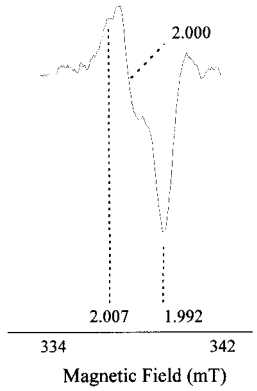

FIGURE 8: EPR difference spectrum at 4 K showing structure on S_{EPR2}. Spectrum was produced by subtracting the signal when C_2D_2 in D_2O was used from the spectrum when C_2H_2 in H_2O was used.

Isotopic substitution has often been used to elucidate a paramagnetic center. For example, EPR spectra of the α-Gln[195] MoFe protein turnover samples containing either $^{13}C_2H_2$ or C_2D_2 show small isotope-induced line width changes (*17*), suggesting that C_2H_2 adducts bind to the FeMo-cofactor to generate S_{EPR1}. This conclusion was confirmed by ^{13}C ENDOR studies that demonstrated that at least two C_2H_2 adducts are bound to the FeMo-cofactor to produce the EPR signal (*18*). To test the possible involvement of solvent with the different species in the C_2H_2-induced signal, the α-Gln[195] MoFe protein was exchanged into buffered D_2O and C_2H_2, and turnover samples were prepared. No isotope-induced line width changes were observed under these conditions, a result consistent with our inability to detect solvent-exchangeable protons in the ^1H ENDOR spectrum (*18*). What is observed in the EPR spectrum is a change in the amplitude ratio $[S_{EPR1}]/[S_{EPR2}]$. Specifically, there is an increase in this ratio for the spectrum of C_2H_2 in H_2O relative to C_2H_2 in D_2O. This solvent isotope effect is unexpected and suggests that one or both of the paramagnetic species are stabilized through hydrogen bonding interactions. Furthermore, because the solvent exchange affects the ratio of the signals but does not affect their shape, subtraction of these spectra can be used to generate the X-band spectrum of S_{EPR2} (Figure 8) and reveals the presence of structure. Better resolution of this structure has recently been recorded at Q-band frequencies (*18*).

Assignment of S_{EPR1} and S_{EPR2}. Spectroscopic data now allow for a proposed identification of the species giving rise to S_{EPR1} and S_{EPR2}. EPR spectra recorded using $^{13}C_2H_2$ and C_2D_2 as substrate show small isotope-induced line width changes of S_{EPR1} consistent with C_2H_2 adducts binding to the FeMo-cofactor (*17*). The lack of similar isotope-induced spectral changes in S_{EPR2} implied that it did not involve C_2H_2. These assignments have now been confirmed by ^{13}C Q-band ENDOR studies using $^{13}C_2H_2$ (*18*) that reveal ^{13}C hyperfine interactions in S_{EPR1} but none in S_{EPR2}. Similarly, both the ENDOR spectrum and the cooperative dependency of the formation of the EPR signal (Figure 6) suggest two C_2H_2 adducts are bound to the FeMo-cofactor. Finally, ^1H ENDOR measurement only detected proton signals originating from C_2H_2 while no solvent-exchangeable proton signals were observed. These results have allowed us to propose that S_{EPR1}

Table 3: *g*-Factors

radical	g_x	g_y	g_z	g_{iso}	ref
S_{EPR2}	2.007	2.000	1.992	2.000	*17*
benzene	2.003	2.003	2.002	2.003	*45*
benzosemiquinone	2.006	2.005	2.002	2.004	*46*
tyrosyl (*E. coli* RDPR)	2.008	2.005	2.002	2.005	*47*
tryptophan (*E. coli* RNR)	2.003	2.003	2.002	2.003	*48*
intermediate X (*E. coli* RNR)	2.007	1.999	1.994	2.000	*37*
hydrogenase (*C. vinosum*)	2.018	2.016	2.002	2.012	*38*
$C_2H_5O\bullet$	2.034	2.007	2.002	2.014	*49*
$CH_3S\bullet$	2.057	2.025	1.997	2.031	*49*
cysteine	2.052	2.025	2.000	2.026	*50*
$CO_2^-\bullet$ (in $NaHCO_3$)	2.003	2.001	1.998	2.001	*51*
NO_2 (in MgO)	2.006	2.002	1.991	1.999	*52*

arises from the binding of two C_2H_2 adducts (C_2H_x) to the FeMo cofactor. One of the adducts is C_2H_2 (i.e., $x = 2$) oriented in a side-on fashion to Fe ions in the waist region of the FeMo-cofactor, while the second adduct (C_2H_x) has not yet been determined.

The S_{EPR2} signal requires C_2H_2 or C_2H_4 (see below) and the α-Gln^{195} protein but is not detected during turnover when only Ar, N_2, or CO is used. Obviously, the former substrates perturb the α-Gln^{195} protein to stabilize this species. The identity of S_{EPR2} can be investigated through a comparison of its spectral parameters with those of known biological paramagnets. The X-band (9.5 GHz) difference spectrum (Figure 8) reveals structure on S_{EPR2} that consists of three peaks with separations of 0.9 and 1.4 mT. When this signal is recorded at Q-band frequencies [35 GHz, (*18*)], these separations increase to 4.2 and 5.2 mT, or about four times those at X-band. Because the increase in separation roughly parallels the increase in irradiating frequency, the structure arises from Zeeman rather than hyperfine interactions, as previously suggested (*17*). Principal *g*-factors of this signal have been assigned [2.007, 2000, 1.992] and can be used to propose the origin of the signal. It is important to note that no hyperfine structure is observed, and the small spread in *g*-factors strongly suggests that S_{EPR2} either originates from a radical species or from an unusual metal cluster. As an example of the latter, intermediate X formed during cofactor assembly in *Escherichia coli* ribonucleotide reductase (*37*) has nearly identical *g*-factors to S_{EPR2} yet involves an oxygen bridged diiron center. EPR spectra from $[Fe_3S_4]^+$ clusters in proteins are fairly isotropic but not as much as S_{EPR2} as exemplified by the spectrum of *Chromatium vinosum* hydrogenase (*38*). Table 3 lists *g*-factors of this species along with other common radicals. The *g*-factors of pure hydrocarbon radicals (e.g., benzene) deviate only slightly from that of the free electron (2.0023) and are almost always greater than that value. On the other hand, sulfur-based radicals can have *g*-factors that deviate significantly from the free electron due to the dominant spin−orbit coupling constant of sulfur. The moderate deviation of the S_{EPR2} *g*-factors from the free electron suggests minor spin−orbit coupling consistent with the radical being nitrogen, carbon, and/or oxygen based, analogous to NO_2 or CO_2^- shown in Table 3. The lack of observable hyperfine structure (e.g., the isotropic hyperfine splitting for ^{14}N in NO_2 is $a = 5.42$ mT) means that this signal does not arise from a nitrogen centered radical and is probably not the substituted glutamine moiety at the α-195 position. Therefore, if S_{EPR2} does not involve a metal center, the most likely candidate for its origin is a carbon and oxygen-containing species such as a carboxylate-centered radical possibly associated with homocitrate or the amino acids glutamate or aspartate. This assignment is further strengthened by the fact that two of the principal *g*-factors of S_{EPR2} have values less than the free electron. This situation often occurs with electron-rich radicals such as a carboxylate which contain low-lying electronic excited states that can mix with the ground state to reduce the effective *g*-factor.

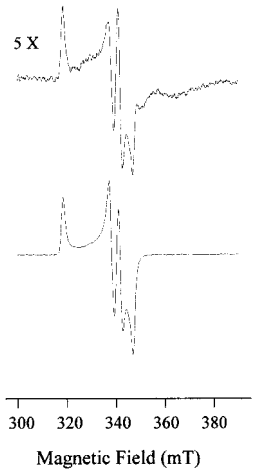

FIGURE 9: EPR spectrum of α-Gln^{195} during turnover in the presence of C_2H_2 (0.1 atm, lower spectrum) and C_2H_4 (1.0 atm, upper spectrum). Note that under these conditions the C_2H_4 spectrum is about 20% of the amplitude of the C_2H_2 spectrum. Spectral parameters are the same as those given in Figure 2, panel B.

Turnover of the α-Gln^{195} MoFe Protein in the Presence of C_2H_4. One of the most interesting finds of this study is that turnover samples containing the α-Gln^{195} MoFe protein in the presence of C_2H_4 also generated an EPR spectrum containing S_{EPR1}, S_{EPR2}, and S_{EPR3}. Initially, this observation was interpreted to suggest that the adducts bound to the FeMo cofactor were C_2H_4. However, recent ENDOR studies reveal that at least one of the bound adducts is C_2H_2. It is, therefore, of interest to further characterize this system.

Although the presence of C_2H_4 allows the generation of the same signals observed with C_2H_2, it is important to note that the two systems are not identical. First, while the C_2H_2-induced spectrum is intense and reaches a maximum at 10% C_2H_2, the C_2H_4-induced spectrum is much weaker and continually grows in intensity up to 100% C_2H_4 without ever reaching a maximum. The C_2H_4 used in these experiments was analyzed and found to have undetectable amounts of C_2H_2 (<0.0025% C_2H_2). Because the production of a comparable EPR signal would require at least 2% C_2H_2 (Figure 6), the C_2H_4-induced signal is not an artifact arising from C_2H_2 contamination. Second, the relative amount of S_{EPR2} in the C_2H_4-induced signal (as compared to S_{EPR1}) is smaller than in the C_2H_2-induced signal (Figure 9). Finally, additional inflections are detected in the C_2H_4-induced spectrum that are not observed in the C_2H_2-induced spectrum. One of these is an $S = 1/2$ signal (termed *g* 2.06) observed at 12 K with *g*-factors [2.06, 1.94, 1.86] when 1.0 atm C_2H_4 is present. The relative intensity of this signal depends on the nitrogenase component ratio (Figure 10). For example, at 12 K and a 1:1 component protein ratio, the *g* 2.06 signal accounts for 10% of the total cofactor concentration and decreases to 2% upon lowering the ratio to 1:5 (the

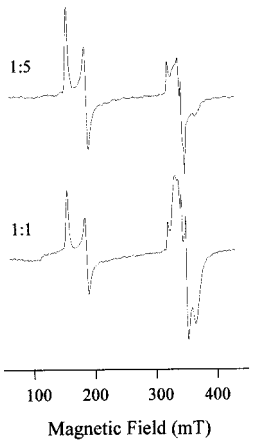

FIGURE 10: Dependence of the EPR spectrum of α-Gln[195] during turnover in the presence of C_2H_4 (1.0 atm) on the [Fe protein]/[MoFe protein] component ratio (1:5 and 1:1). At the higher ratio (1:1), the *g* 2.06 signal, putatively identified as the reduced Fe protein, becomes dominant. Notice also the relatively large contribution from the $S = 3/2$ FeMo-cofactor signal. Spectral parameters are the same as those used in Figure 2, panel A.

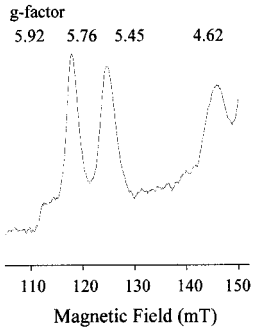

FIGURE 11: Low-field $6 \geq g \geq 4$ region of the EPR spectrum of α-Gln[195] in the presence of C_2H_4 (1.0 atm) recorded at 4 K. All four inflections decreased with increasing temperature suggesting that each signal represents the ground-state transitions of a different $S = 3/2$ spin system.

concentrations of the other signals are unaffected by this change in ratio). This signal is typical of an $S = 1/2$ FeS-cluster being easily saturated at high powers and low temperature (4 K) leaving only the signal corresponding to the C_2H_2-induced species (Figure 9).

At 4 K, additional inflections at $g = 5.92$, 5.76, 5.45, and 4.62 (Figure 11) are detected. The range of *g*-factors for these inflections ($6 \geq g \geq 4$) implies that they are associated with $S = 3/2$ spin states, and temperature-dependence studies show that they all represent ground-state transitions. The magnitude of the axial zero-field splitting terms (*D*) for these signals could not be measured due to spectral overlap but is obviously < 0 for the first two inflections and > 0 for the last inflection (Table 2). The three dominant inflections ($g = 5.76$, 5.45, and 4.62) are similar to those previously observed by Lowe et al. (*15*) in turnover samples of *Klebsiella pneumoniae* under Ar or C_2H_2 (but not under C_2H_4). Therefore, these low-field inflections presumably represent general turnover states of the enzyme.

Effect of C_2H_4 on Proton Reduction. The ability of C_2H_4 to inhibit the reduction of protons was examined by measuring hydrogen evolution catalyzed by the α-Gln[195] MoFe protein under either an C_2H_4 or Ar atmosphere. Hydrogen evolution specific activity for a 1:5 [Fe protein]/[MoFe protein] component ratio was found to be inhibited by 33% under a C_2H_4 atmosphere when compared to an identical sample under an Ar atmosphere. This inhibition increased to 40% when the component ratio was raised to 1:1. These data are in agreement with another recently reported study on the α-Gln[195] MoFe protein (*32*). In that work, it was reported that C_2H_4 inhibits electron flux without uncoupling MgATP hydrolysis from electron transfer. Our results involving turnover samples prepared under C_2H_4 provide insight on this issue. As mentioned above, under our experimental conditions, an $S = 1/2$ *g* 2.06 is observed. The *g*-factors of this signal suggest that it could arise from a mixture of reduced Fe protein in the free ($g = [2.05, 1.94, 1.88]$) and nucleotide-bound ($g = [2.03, 1.92, 1.92]$) forms. Consistent with this interpretation, the intensity of the signal increases with the relative concentration of the Fe protein (Figure 10). In contrast, parallel turnover samples prepared under an Ar atmosphere exhibited very little signal from the Fe protein, most of which is in the $S = 0$ oxidized state as a result of electron transfer to the MoFe protein. The simultaneous detection of a significant concentration of the reduced Fe protein and the $S = 3/2$ FeMo-cofactor EPR signal in the high $P_{C_2H_4}$ turnover sample suggests that electron transfer is inhibited by high levels of C_2H_4. In other words, during turnover under an Ar atmosphere, most of the Fe protein has transferred an electron to the MoFe protein, thus reducing the FeMo-cofactor to an EPR-silent state and leaving the Fe protein in an EPR-silent oxidized form. However, under identical turnover conditions but in the presence of high $P_{C_2H_4}$, a larger fraction of the FeMo-cofactor is in the $S = 3/2$ resting state and a significant portion of the Fe protein is in a $S = 1/2$ reduced form. Because MgATP hydrolysis is not uncoupled from electron transfer, we interpret these results to indicate that C_2H_4 inhibits MoFe protein activity by preventing component protein association.

Crystal Structure of α-Gln[195] MoFe Protein. We also investigated whether there was a structural interpretation of our results. The structure of the α-Gln[195] MoFe protein was determined by X-ray diffraction methods and refined to 2.5 Å resolution with a R_{cryst} of 18.2% (Table 1). In the wild-type structure the α-His[195] residue provides one of three NH−S hydrogen-bonding interactions that occur at each of the bridging S atoms of the FeMo-cofactor (*39*). Specifically, the Nϵ atom of α-His[195] imidazole side-chain is hydrogen bonded to a bridging sulfur atom, whereas the Nδ atom of that group is hydrogen bonded to a solvent water molecule, which in turn is hydrogen bonded to α-Tyr[281] and α-Ser[192] (Figure 1). The structure of the α-Gln[195] MoFe protein reveals that the hydrogen bond interaction between the Nϵ of α-His[195] and the FeMo-cofactor bridging S has been replaced by an analogous interaction by glutamine with the same S atom (Figure 1). It cannot be determined from the crystallographic model whether it is the Oϵ or Nϵ of the glutamine side-chain that approaches the bridging S atom. However, we consider it unlikely that the Oϵ provides the hydrogen bond because substitution of α-His[195] by glutamate results in accumulation of a primarily cofactorless MoFe protein. The structure of the α-Gln[195] MoFe protein also shows that the water molecule stabilizing the position of the α-His[195] side chain via α-Tyr[281], α-Ser[192], and the carbonyl oxygen of α-Arg[277] in the wild type enzyme is absent in the altered protein. However, the assignment of solvent molecules

reliably at the current resolution (2.5 Å) is difficult and such disruption is likely to have only very minor effects, if any, because altered MoFe proteins substituted by asparagine, threonine, glycine, leucine, or valine at the α-Ser^{192} position remain capable of effective dinitrogen reduction. Other than the changes described above, and also shown in Figure 1, the α-Gln^{195} MoFe protein structure is essentially superimposable upon the wild-type MoFe protein. Thus, the structural determination reported here is in good agreement with our previous conclusion, based on electron spin−echo envelope modulation (*31*). Namely, the functional and spectroscopic perturbations recognized for the α-Gln^{195} MoFe protein are likely to specifically arise from loss of the imidazole group as the source of hydrogen bonding to the bridging S atom of FeMo-cofactor rather than from indirect structural changes within the first shell of FeMo-cofactor−polypeptide interactions.

SUMMARY

The wild-type MoFe protein does not exhibit a new EPR signal when incubated under turnover conditions in the presence of C_2H_2. In contrast, the α-Gln^{195} MoFe protein does exhibit three readily detected signals when incubated under these same conditions. Kinetic studies have shown that the wild type and α-Gln^{195} MoFe have the same K_m values, but the α-Gln^{195} MoFe exhibits a modestly lower V_{max} (*13*). Thus, a slower product release rate is a reasonable explanation for the appearance of an C_2H_2-induced EPR signal in the case of the α-Gln^{195} MoFe protein. Comparison of a crystallographically determined structure for the α-Gln^{195} MoFe protein to the wild-type MoFe protein model indicates that spectroscopic and catalytic perturbations caused by the α-Gln^{195} substitution can be attributed specifically to the loss of an imidazole group as a source of NH−S hydrogen bonding to the FeMo-cofactor.

A pathway for the binding and reduction of C_2H_2 can be considered on the basis of data reported here and elsewhere (*18*). Previous kinetic data show that C_2H_2 does not bind to the cofactor until it is one or two electrons reduced (*40*). Past studies on C_2H_2 interaction with transition metals indicate that it almost always undergoes σ-bonding to the transition metal with π-back-bonding in a preferred side-on perpendicular orientation (although parallel bonding can also occur) (*41*). If the initial binding of C_2H_2 to the FeMo-cofactor does occur in a perpendicular orientation then a rotational shift of C_2H_2 to a side-on parallel bridging orientation, as indicated by the ENDOR study (*18*), is necessary. Molecular orbital calculations indicate that this rotation could have a high activation energy (*42*, *43*). The source of energy required for this rotation to occur during nitrogenase catalysis is not known but could be related to protein conformational changes elicited by component protein interaction (*44*) or redox state (*3*). Such an event is also likely to be affected by specific interactions with amino acids within the first shell of noncovalent interaction with FeMo-cofactor. Regardless, subsequent protonation of the reduced cofactor-bound C_2H_2 species (S_{EPR1}) would result in the release of an C_2H_4 molecule. A remarkable finding from the present work is that this last protonation step is apparently reversible, as illustrated by the ability of C_2H_4 to elicit S_{EPR1}. Such a transition metal deprotonation of C_2H_4 might be unique to the protein/cofactor structure and interaction found in nitrogenase.

REFERENCES

1. Burgess, B. K., and Lowe, D. J. (1996) *Chem. Rev. 96*, 2983−3011.
2. Georgiadis, M. M., Komiya, H., Chakrabarti, P., Woo, D., Kornuc, J. J., and Rees, D. C. (1992) *Science 257*, 1653−1659.
3. Peters, J. W., Stowell, M. H. B., Soltis, M. S., Finnegan, M. G., Johnson, M. K., and Rees, D. C. (1997) *Biochemistry 36*, 1181−1197.
4. Burgess, B. K. (1990) *Chem. Rev. 90*, 1377−1406.
5. Kim, J., and Rees, D. C. (1992) *Science 257*, 1677−1682.
6. Yates, M. G. (1991) in *Biological Nitrogen Fixation* (Stacey, G., Burris, R. H., and Evans, H. J., Eds.) pp 685−735, Chapman and Hall, New York.
7. Burris, R. H. (1979) in *A Treatise on Dinitrogen Fixation, Sections I and II: Inorganic and Physical Chemistry and Biochemistry* (Hardy, R. W. F., Bottemely, F., and Burns, R. C., Eds.) pp 569−604, John Wiley and Sons, Inc., New York.
8. Burgess, B. K. (1985) in *Nitrogen Fixation Research Progress* (Evans, H. E., Bottomley, P. J., and Newton, W. E., Eds.) pp 543−550, Martinus Nijhoff, Dordrecht.
9. Dean, D. R., Bolin, J. T., and Zheng, L. (1993) *J. Bacteriol. 175*, 6737−6744.
10. Seefeldt, L. C., and Dean, D. R. (1997) *Acc. Chem. Res. 30*, 260−266.
11. Orme-Johnson, W. H. (1985) *Annu. Rev. Biophys. Chem. 14*, 419−459.
12. Shah, V. K., and Brill, W. J. (1977) *Proc. Natl. Acad. Sci. U.S.A. 74*, 3249−3253.
13. Kim, C.-H., Newton, W. E., and Dean, D. R. (1995) *Biochemistry 34*, 2798−2808.
14. Yates, M. G., and Lowe, D. J. (1976) *FEBS Lett. 72*, 121−126.
15. Lowe, D. J., Eady, R. R., and Thorneley, R. N. F. (1978) *Biochem. J. 173*, 277−290.
16. Davis, L. C., Henzl, M. T., Burris, R. H., and Orme-Johnson, W. H. (1979) *Biochemistry*, 4860−4869.
17. Sørlie, M., Christiansen, J., Dean, D. R., and Hales, B. J. (1999) *J. Am. Chem. Soc. 121*, 9457−9458.
18. Lee, H.-I., Sørlie, M., Christiansen, J., Song, R., Dean, D. R., Hales, B. J., and Hoffman, B. M. (2000) *J. Am. Chem. Soc., 122*, 5582−5587.
19. Scott, D. J., Dean, D. R., and Newton, W. E. (1992) *J. Biol. Chem. 267*, 20002−20010.
20. Strandberg, G. W., and Wilson, P. W. (1968) *Can. J. Microbiol. 14*, 25−31.
21. Burgess, B. K., Jacobs, D. B., and Stiefel, E. I. (1980) *Biochim. Biophys. Acta 614*, 196−209.
22. Christiansen, J., Goodwin, P. J., Lanzilotta, W. N., Seefeldt, L. C., and Dean, D. R. (1998) *Biochemistry 37*, 12611−12623.
23. Chromy, V., Fischer, J., and Kulhanek, V. (1974) *Clin. Chem. 20*, 1362−1363.
24. Laemmli, U. K. (1970) *Nature 227*, 680−685.
25. Aasa, R., and Vänngård, T. (1975) *J. Magn. Reson. 19*, 308−315.
26. Tittsworth, R. C., and Hales, B. J. (1993) *J. Am. Chem. Soc. 115*, 9763−9767.
27. Hagen, W. R. (1992) in *Advances in Inorganic Chemistry: Iron−Sulfur Proteins* (Sykes, A. G., and Cammack, R., Eds.) pp 165−222, Academic Press.
28. Otwinowski, Z. (1993) in *Data Collection and Processing* (Sawyer, L., Issacs, N., and Bailey, S., Eds.) pp 56−62, SERC Darebury Laboratory, Daresbury.
29. Jones, T. A., Zou, J. Y., Cowan, S. W., and Kjeldgaard, M. (1991) *Acta Crystallog. Sect. D 47*, 110−119.
30. Brünger, A. T., Kuriyan, J., and Karplus, M. (1987) *Science 235*, 458−460.
31. DeRose, V. J., Kim, C.-H., Newton, W. E., Dean, D. R., and Hoffman, B. M. (1995) *Biochemistry 34*, 2809−2814.

32. Fisher, K., Dilworth, M. J., Kim, C. H., and Newton, W. E. (2000) *Biochemistry 39*, 2970−2979.
33. Dilworth, M. J., Fisher, K., Kim, C. H., and Newton, W. E. (1998) *Biochemistry 37*, 17495−505.
34. Cameron, L. M., and Hales, B. J. (1998) *Biochemistry 37*, 9449−56.
35. Surerus, K. K., Hendrich, M. P., Christie, P. D., Rottgardt, D., Orme-Johnson, W. H., and Münck, E. (1992) *J. Am. Chem. Soc. 114*, 8579−8590.
36. Pierik, J., Wassink, H., Haaker, H., and Hagen, R. (1993) *Eur. J. Biochem. 212*, 51−61.
37. Sturgeon, B. E., Burdi, D., Chen, S., Huynh, B.-H., Edmondson, D. E., Stubbe, J., and Hoffman, B. M. (1996) *J. Am. Chem. Soc. 118*, 7551−7557.
38. Surerus, K. K., Chen, W., Zwaan, W., Rusnak, F. M., Kolk, M., Duin, E. C., Albracht, S. P. J., and Münck, E. (1994) *Biochemistry 33*, 4980−993.
39. Kim, J., and Rees, D. C. (1992) *Nature 360*, 553−560.
40. Lowe, D. J., Fisher, K., and Thorneley, R. N. F. (1990) *Biochem. J. 272*, 621−625.
41. Amouri, H. E., and Gruselle, M. (1996) *Chem. Rev. 96*, 1077−1103.
42. Hoffman, D. M., Hoffman, R., and Fisel, C. R. (1982) *J. Am. Chem. Soc. 104*, 3858−3875.
43. Pepermans, H., and Hogzand, C. (1986) *J. Organomet. Chem. 306*, 395−405.
44. Howard, J. B., and Rees, D. C. (1996) *Chem. Rev. 96*, 2965−2982.
45. Stone, A. J. (1963) *J. Mol. Phys. 6*, 509−515.
46. Hales, B. J. (1975) *J. Phys. Chem.* 5993−5997.
47. Un, S., Tang, X.-S., and Diner, B. A. (1996) *Biochemistry 35*, 679−684.
48. Lendzian, F., Sahlin, M., MacMillian, F., Bittl, R., Fiege, R., Pötsch, S., Sjöberg, B.-M., Gräslund, A., Lubitz, W., and Lassmann, G. (1996) *J. Am. Chem. Soc. 118*, 8111−8120.
49. Sullivan, P. J., and Koski, W. S. (1964) *J. Am. Chem. Soc. 86*, 159−162.
50. Windle, J. J., and Wiersema, A. K. (1996) *J. Chem. Phys. 41*, 1996−2002.
51. Ovenall, D. W., and Whiffen, D. H. (1961) *Mol. Phys. 4*, 135.
52. Zeldes, H., and Livingston, R. (1961) *J. Chem. Phys. 35*, 563−567.

BI0013997